Hindawi Publishing Corporation
Journal of Chaos
Volume 2014, Article ID 429809, 15 pages
http://dx.doi.org/10.1155/2014/429809

Research Article

Theoretical Analysis and Adaptive Synchronization of a 4D Hyperchaotic Oscillator

T. Fonzin Fozin,[1,2] J. Kengne,[2,3] and F. B. Pelap[1]

[1] *Laboratoire de Mécanique et de Modélisation des Systèmes Physiques (L2MSP), Faculty of Science, University of Dschang, P.O. Box 69 Dschang, Cameroon*
[2] *Laboratoire d'Electronique et de Traitement de Signal (LETS), Faculty of Science, University of Dschang, P.O. Box 67 Dschang, Cameroon*
[3] *Laboratoire d'Automatique et Informatique Appliquée (LAIA), IUT-FV Bandjoun, University of Dschang, P.O. Box 67 Dschang, Cameroon*

Correspondence should be addressed to F. B. Pelap; fbpelap@yahoo.fr

Received 31 October 2013; Accepted 14 January 2014; Published 27 February 2014

Academic Editor: Qingdu Li

We propose a new mathematical model of the TNC oscillator and study its impact on the dynamical properties of the oscillator subjected to an exponential nonlinearity. We establish the existence of hyperchaotic behavior in the system through theoretical analysis and by exploiting electronic circuit experiments. The obtained numerical results are found to be in good agreement with experimental observations. Moreover, the new technique on adaptive control theory is used on our model and it is rigorously proven that the adaptive synchronization can be achieved for hyperchaotic systems with uncertain parameters.

1. Introduction

Over the last four decades, an increasing interest has been shown on chaotic systems with higher dimensional attractors known as hyperchaotic. The interest for hyperchaotic dynamics is justified by the rapid development of new techniques in various areas of physics such as nonlinear circuits [1–6], complex system studies [7, 8], laser dynamics [9–11], secure communication [12, 13], and synchronization [14–21]. Hyperchaotic systems are usually classified as chaotic systems with more than one positive Lyapunov exponent, indicating that the chaotic dynamics of the systems are expanded in some directions but rapidly shrink in other directions, which significantly increase the system's orbital degree or disorder and randomness. Those systems are suitable for engineering application such as secure communications [12–14, 19, 20, 22]. In fact, in 1995, Pérez and Cerdeira [23] have shown that by masking signals with simple chaos with only one Lyapunov exponent does not provide high level of security. Hence, the use of more complex hyperchaotic signals is a straightforward way to overcome this limitation because of their increased randomness and higher unpredictability [24]. Therefore the dynamical behavior of several hyperchaotic electronic circuits has been studied [1, 2, 4–6, 10, 11, 25–27]. Within these, TNC oscillator [2] retains our attention. Indeed, it is extremely simple and provides a powerful tool for understanding the inherent architectures and dynamical behavior of hyperchaotic oscillator as well as their use as chaotic carriers in practical secure communication. Its synchronization and dynamics have been studied using a piecewise linear (PWL) model [4, 28]. Moreover, Peng et al. in [14], address the synchronization of hyperchaotic oscillators using a scalar transmitted signal. Furthermore, this scalar synchronization does not require either the computation of the Lyapunov exponent or initial conditions belonging to the same basin of attraction. For a possible use of hyperchaotic behavior in secure communication, the synchronization of hyperchaotic systems via a single dynamical variable is demonstrated [20, 29, 30]. In 2001, Miller and Grassi [19] described an experimental realization of observer-based hyperchaos synchronization using the TNC oscillator [31]. X. Wang and Y. Wang in [29] deal with the synchronization

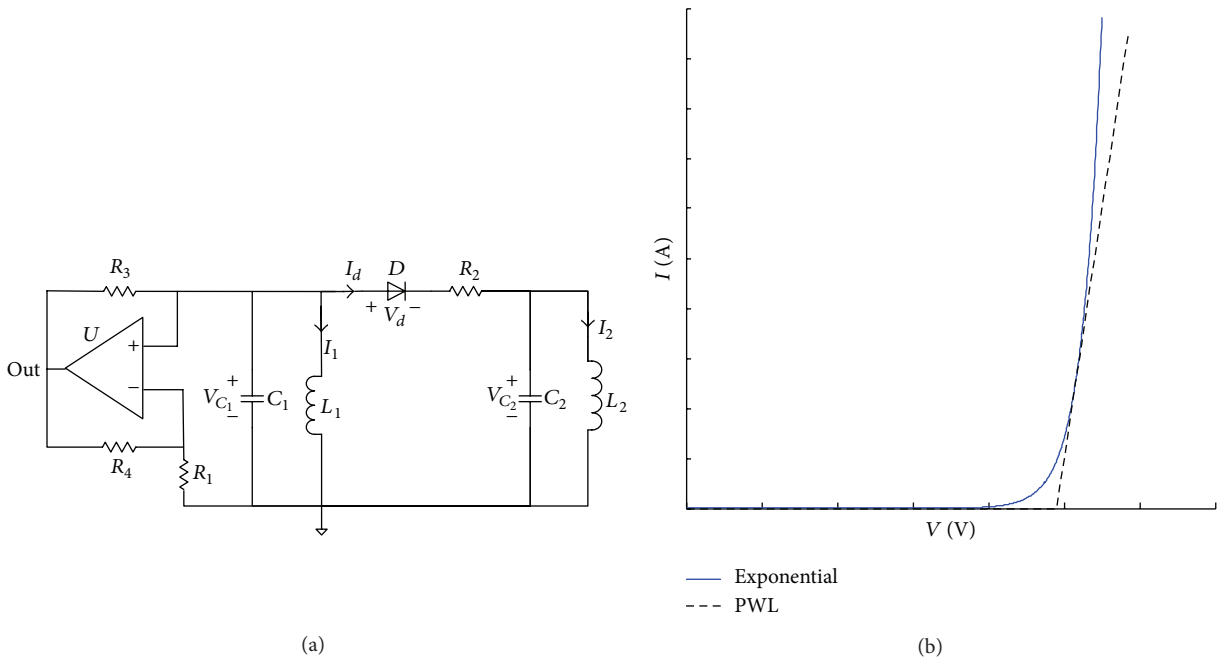

FIGURE 1: (a) Schematic diagram of the modified TNC hyperchaotic oscillator. The operational amplifier with feedback resistors R_1, R_3, and R_4 acts both as the negative impedance converter (NIC) and the output amplifier. (b) Current-voltage characteristic showing the exponential and the PWL models of the diode.

of uncertain hyperchaotic and chaotic systems by adaptive control using the TNC hyperchaotic oscillator as the master and the Rössler oscillator as the slave. However, the aforementioned analysis is performed based on the piecewise linear model of the system. Furthermore, to our knowledge, no design tool exist that may be exploited for design purposes of a Tamasevicius oscillator built by Grassi and Mascolo [4]. In fact, the PWL model represents only a first-order approximation of the reality and therefore may give rise to different types of bifurcation compared to those exhibits by the real oscillator. Moreover, Kengne et al. [32, 33] derive smooth mathematical model instead of PWL to perform the analysis of the two-stage Colpitts oscillator and the improved Colpitts oscillator. They also synchronize those coupled oscillators (with smooth mathematical model) using nonlinear state observers. Using the same concept, we propose in this paper a new smooth (exponential) mathematical model to investigate the nonlinear dynamics of the TNC oscillator. We address two key issues. The first is to point out both theoretical and experimental tools, which may be exploited for design and control purposes. The second is to complete the results obtained so far by deriving a mathematical model from which a systematic and methodological analysis of the nonlinear dynamics of the oscillator is carried out helping to point out some unknown and striking behavior of the TNC oscillator.

The organization of the paper is as follows. Section 2 deals with the modeling process. The electronic structure of the oscillator is presented and the appropriate mathematical model is derived to describe the dynamic behavior of the oscillator. The stability analysis of the equilibrium point and local bifurcation is presented in Section 3. The evolution process analysis by means of Lyapunov exponent spectrum, bifurcation diagram, and phase portraits is investigated in Section 4, where numerical simulations studies are given. In Section 5, an experimental study is carried out. The corresponding electronic circuit is implemented, exhibiting experimental chaotic attractors in accord with numerical simulations which serves to validate the model derived in this work. Section 6 considers the synchronization of such type of oscillators. By exploiting recent results on adaptive control theory, a controller is designed that combines the synchronization of two one-way coupled systems and the estimation of unknown parameters of the drive system. Finally the summary of the results is given in Section 7.

2. Circuit Description and Mathematical Model

2.1. Circuit Description. The model under consideration is the electronic oscillator of the Tamasevicius, Namajuas, and Cenys (TNC) given by Figure 1(a). It consists of a combined parallel-series LC circuit (namely, L_1C_1-L_2C_2), a single operational amplifier (op amp) with feedback resistors R_1, R_3, R_4 implementing both the negative impedance (NIC) and the output amplifier for the oscillator with a diode. This diode is the nonlinear device responsible for the hyperchaotic behavior of the oscillator. One should note that as the op amp operates in the linear region for $R_3 = R_4$, the input impedance of the NIC satisfies $R = -R_1$ and the output obeys $V_{\text{out}} = (1 + R_4/R_3)V_{C_1}$.

2.2. Mathematical Model. This subsection introduces the new mathematical model of the TNC oscillator by considering the following hypotheses. Firstly, we assume that all capacitors, inductors, and resistors of the oscillator network are linear. Secondly, the current-voltage (I-V) characteristic of the diode D is modeled with an exponential function (Figure 1(b)) [34] as yields in

$$I_d = f\left(V_d\right) = I_s\left[\exp\left(\frac{V_d}{\eta V_T}\right) - 1\right] \tag{1}$$

in which V_d is the voltage drop across the diode, I_s represents the saturation current of the junction, η stands for the ideality factor ($1 < \eta < 2$), and $V_T = k_b T/q$ is the thermal voltage wherein k_b is the Boltzmann constant, T the absolute temperature expressed in Kelvin, and q the electron charge. Let us note that at room temperature (300 K), we have $V_T \approx 26$ mV. If we denote by I_n ($n = 1, 2$) the current flowing through the inductor L_n and V_{C_m} ($m = 1, 2$) the voltage across capacitor C_m, the Kirchhoff's electric circuit laws can be applied on Figure 1(a) to obtain the upcoming set of autonomous differential equations describing the dynamics of the TNC hyperchaotic oscillator:

$$\frac{dI_1}{dt} = \frac{V_{C_1}}{L_1}, \tag{2a}$$

$$\frac{dI_2}{dt} = \frac{1}{L_2}\left(V_{C_1} - V_d - R_2 I_d\right), \tag{2b}$$

$$\frac{dV_{C_1}}{dt} = \frac{1}{C_1}\left(\frac{V_{C_1}}{R} - I_1 - I_d\right), \tag{2c}$$

$$\frac{dV_d}{dt} = \frac{\left(V_{C_1} - I_1 - I_d\right)/C_1 - \left(I_d - I_2\right)/C_2}{1 + R_2 dI_d/dV_d}, \tag{2d}$$

where the diode current I_d is defined by (1). In contrast to previous literature [2, 4, 31] based on PWL models of the TNC oscillator, the exponential model is considered in this paper. Indeed, the PWL model is only its first-order approximation and can approximately match only over a limited region (Figure 1(b)) and, thus, may exhibit different types of bifurcation compared to the exponential model as previously mentioned. Furthermore, owing to the fact that a smooth mathematical model is more tractable both analytically and numerically, it may be exploited to obtained exact bifurcation structures occurring in the real TNC hyperchaotic oscillator circuit. It is worth mentioning that the bifurcation diagrams are very useful for design purpose as they allow the selection of the right parameters settings giving rise to a regular or erratic behavior (hyperchaotic mode of operation). For computer simulation, we normalize the state equations (2a)–(2d) by considering the following rescaled variables and parameters:

$$x = \frac{\rho I_1}{\eta V_T}; \quad y = \frac{\rho I_2}{\eta V_T}; \quad z = \frac{V_{C_1}}{\eta V_T};$$

$$w = \frac{V_d}{\eta V_T}; \quad \rho = \sqrt{\frac{L_1}{C_1}}; \quad \tau = \frac{t}{\sqrt{L_1 C_1}};$$

$$\varepsilon_1 = \frac{L_1}{L_2}; \quad \gamma = \frac{R_2 I_s}{\eta V_T}; \quad \sigma = \frac{\rho}{R_1}; \quad \alpha = \frac{\rho I_s}{\eta V_T};$$

$$\varepsilon_2 = \frac{C_1}{C_2}. \tag{3}$$

Therefore, we obtain the upcoming smooth normalized fourth-order differential equations:

$$\dot{x} = z, \tag{4a}$$

$$\dot{y} = \varepsilon_1\left(z - w - \gamma\varphi\left(w\right)\right), \tag{4b}$$

$$\dot{z} = \sigma z - x - \alpha\varphi\left(w\right), \tag{4c}$$

$$\dot{w} = \frac{\sigma z - x - \alpha\varphi\left(w\right) - \varepsilon_2\left(\alpha\varphi\left(w\right) - y\right)}{1 + \gamma\left(\varphi\left(w\right) + 1\right)} \tag{4d}$$

with

$$\varphi\left(w\right) = \exp\left(w\right) - 1, \tag{4e}$$

where the dots denote differentiation with respect to τ (renamed as t in the new scale without loss of generality). System (4a)–(4d) present only one nonlinear term and one state variable (namely, w) is involved in exponential function. The presence of such exponential nonlinearity implies the nonsymmetry of our model. Therefore, the system cannot support symmetric orbits.

3. Stationary Point and Its Nature

The notion of fixed points in the state space plays a crucial role in understanding the dynamics of nonlinear systems. The equilibria of the system (4a)–(4d) can be calculated by solving the following algebraic equations simultaneously:

$$0 = z, \tag{5a}$$

$$0 = \varepsilon_1\left(z - w - \gamma\varphi\left(w\right)\right), \tag{5b}$$

$$0 = \sigma z - x - \alpha\varphi\left(w\right), \tag{5c}$$

$$0 = \frac{\sigma z - x - \alpha\varphi\left(w\right) - \varepsilon_2\left(\alpha\varphi\left(w\right) - y\right)}{1 + \gamma\left(\varphi\left(w\right) + 1\right)}. \tag{5d}$$

Computation of (5a)–(5d) shows that the origin $O(0, 0, 0, 0)^T$ is the only equilibrium point of the system. By linearizing the system at that equilibrium point, the following 4×4 Jacobean matrix is obtained:

$$M_J = \begin{bmatrix} 0 & 0 & 1 & 0 \\ 0 & 0 & \varepsilon_1 & -\varepsilon_1 A_4 \\ -1 & 0 & \sigma & -\alpha \\ \dfrac{-1}{A_4} & \dfrac{\varepsilon_2}{A_4} & \dfrac{\sigma}{A_4} & \dfrac{-\alpha\left(1 + \varepsilon_2\right)}{A_4} \end{bmatrix}. \tag{6}$$

Then, the eigenvalues associated with this matrix are obtained by solving the following characteristic equation:

$$A_4\lambda^4 + A_3\lambda^3 + A_2\lambda^2 + A_1\lambda + A_0 = 0 \tag{7}$$

with

$$\begin{aligned} A_4 &= 1+\gamma, \qquad A_3 = \alpha(\varepsilon_2+1) - \sigma(1+\gamma), \\ A_2 &= (1+\gamma)(\varepsilon_1\varepsilon_2+1) - \alpha\varepsilon_2\sigma, \\ A_1 &= \alpha\varepsilon_2(1+\varepsilon_1) - \sigma\varepsilon_1\varepsilon_2(1+\gamma), \\ A_0 &= \varepsilon_1\varepsilon_2(1+\gamma). \end{aligned} \tag{8}$$

For the chosen parameters as $\sigma = 0.65$, $\varepsilon_1 = 3$, $\varepsilon_2 = 3.226$, $\alpha = 5.249 \cdot 10^{-5}$,and $\gamma = 5.249 \cdot 10^{-6}$ the eigenvalues solutions of the characteristic equations (7) computed using MATHEMATICA software package are $\lambda_{1,2} = 0.3249 \pm 0.9457i$ and $\lambda_{3,4} = -8.7569 \cdot 10^{-5} \pm 3.1109i$. Since the eigenvalues are complex conjugate with some positive real parts, the equilibrium point $O(0,0,0,0)^T$ is an unstable saddle focus. Physically, this result supports the fact that the oscillator can oscillate chaotically and excludes the existence of stable fixed point motion in the system.

4. Bifurcation Analysis

In order to define different routes/cascades to chaos in our model, system (4a)–(4d) is solved numerically through the fourth-order Runge-Kutta integration algorithm. For each set of parameters used in this work, the time step is always $\Delta t \leq 0.005$ and the simulations are done with variables and constant parameters in extended mode. For each case, the system (4a)–(4e) is integrated for a sufficiently long time and the transient is discarded. Here, two indicators are combined to identify the type of transition which leads to chaos. The first one deals with the bifurcation diagram and the second is related to the Lyapunov exponent's spectra. According to Wolf et al. [35] method, the dynamics of the nonlinear system (4a)–(4e) can be classified in terms of the Lyapunov exponents λ_i $(i = 1, 2, 3, 4)$ as

(1) for an equilibrium point, $\lambda_{1,2,3,4} < 0$;

(2) for a limit cycle (periodic orbits), $\lambda_1 = 0, \lambda_{2,3,4} < 0$;

(3) for 2-torus (quasiperiodic orbits), $\lambda_{1,2} = 0, \lambda_{3,4} < 0$;

(4) for 3-torus, $\lambda_{1,2,3} = 0, \lambda_4 < 0$;

(5) for a chaotic orbits, $\lambda_1 > 0, \lambda_2 = 0,$ and $\lambda_{3,4} < 0$;

(6) for hyperchaotic orbits, $\lambda_{1,2} > 0, \lambda_3 = 0,$ and $\lambda_4 < 0$;

In the next two subsections, the evolution process of the system is analyzed precisely by the means of the Lyapunov exponent's spectrum, bifurcation diagrams, and phase portraits when varying the parameters σ and ε_1 in system (4a)–(4e).

4.1. Influence of σ with Fix ε_1. When the control parameter σ varies in the range [0.25–0.68], the graph of the bifurcation diagrams and its corresponding Lyapunov exponent spectrum are depicted, respectively, in Figures 2 and 3. Each bifurcation diagram is obtained by plotting the local maxima of the related state variable in terms of the control state parameter. In the light of Figures 2 and 3, the following scenarios emerge when monitoring the control parameter σ: periodic $\rightarrow$ quasiperiodic $\rightarrow$ chaos $\rightarrow$ hyperchaos $\rightarrow$ chaos $\rightarrow$ periodic $\rightarrow$ hyperchaos $\rightarrow$ periodic $\rightarrow$ hyperchaos. In other word, they are many windows of hyperchaotic behavior with respect to the control parameter σ. Also, in contrast with the traditional approach which consists of plotting the bifurcation diagram of a single state variable, we have plotted the bifurcation diagram of all the state variables because of the nonuniformity observed between those diagrams. In fact, it can be seen that in the periodic windows, each state variable cycle has a different frequency. However, all state variables share common bifurcation point in terms of the control parameter. In particular, a good coincidence is observed between band of chaos and windows of regular behavior within those diagrams.

Moreover, for the set of parameters of Figure 2, various numerical computations of the phase space trajectories of the system (4a)–(4e) are obtained (Figure 4) confirming transitions to hyperchaos. Those curves represent the phase portraits and their corresponding frequency spectrum computed for some discrete values of σ: periodic oscillations $\rightarrow$ torus state $\rightarrow$ periodic oscillations $\rightarrow$ chaotic oscillations $\rightarrow$ hyperchaotic dynamics. This scenario is in conformity with the bifurcation diagram of Figure 2.

One should note that some new periodic (σ = [0.38–0.42]) windows and some routes to chaos were only observed by using the exponential model of the diode instead of PWL model which is only its first approximation. The simulation results of the model proposed in [2] for exponential and piecewise-linear models are depicted in bifurcation diagram of Figure 5. The observe differences are mainly due to the poor PWL approximation of the exponential characteristic (Figure 1(b)). On the other hand, the nonsmooth nature of the piecewise-linear model of the diode can be responsible for the different bifurcation structure exhibited by our model and the one proposed in [2] as their *I-V* characteristics are not matching perfectly.

4.2. Influence of ε_1 with Fix σ. As can be seen from the bifurcation diagram (Figure 6) and the Lyapunov exponents spectrum (Figure 7), the system (4a)–(4e) can be hyperchaotic, chaotic, and periodic when varying ε_1 in the range [3–8.5]. By observing Figures 3 and 7, it appears that the hyperchaotic range is much wider for ε_1 variation than when σ varies.

A better understanding of the transition from regular oscillations to hyperchaos could be used to achieve more effective control of chaos and also provide some novel ways of the design using such oscillators.

Although the bifurcation analysis was restricted in this work on the effects of parameters σ and ε_1, it is worth mentioning that any other parameters which appear in the

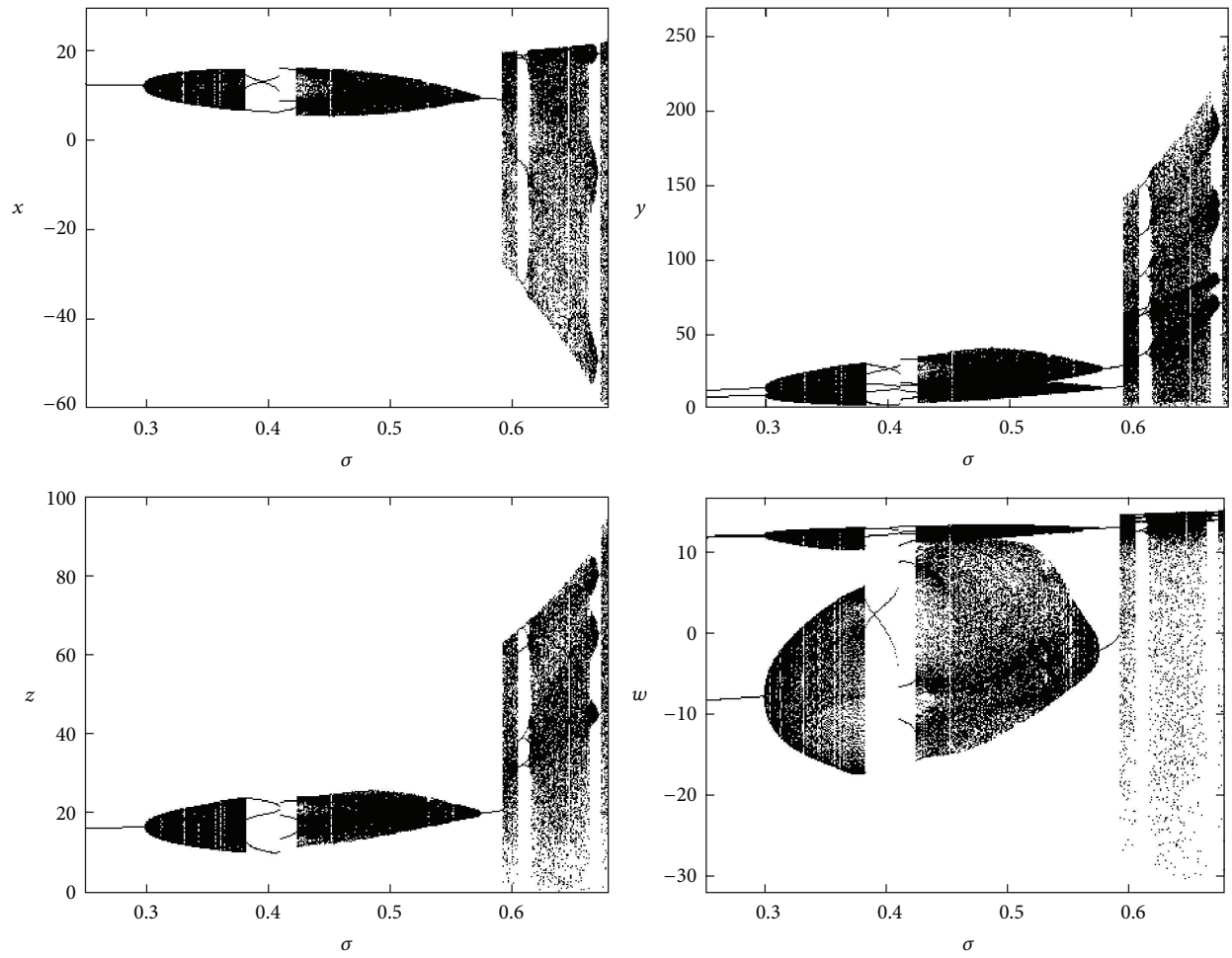

Figure 2: Bifurcation diagrams showing the coordinates x, y, z, and w in terms of the control parameter σ. The others system parameters are $\varepsilon_1 = 3.0$, $\varepsilon_2 = 3.226$, $\gamma = 5.429 \cdot 10^{-6}$, and $\alpha = 5.429 \cdot 10^{-5}$.

characteristic equation could serve as a bifurcation control parameter for the TNC system.

5. Experimental Study

Due to the real-time character of its results, compared to the problems of transient phase duration and numerical instabilities or time steps inherent to numerical simulations, experimental study appears as a complementary technique to the methods mentioned above. Moreover, it is of interest to evaluate the influences of the simplifying process on the real behavior of the oscillator.

5.1. Design of the Experimental Circuit. The circuit diagram of the TNC oscillator depicted in Figure 8 consists of an op. amp (TL082) powered by a symmetric ±12 V DC voltage supply, inductors ($L_1 \sim L_2$) implemented using gyrators [36], capacitors ($C_1 \sim C_2$), resistors (R_1, R_3, and R_4), and a diode D ($1N4148$) ($V_D = 0.65$ V and $R_d = 100\,\Omega$ at 5 mA) in series with its resistor R_d. In the diagram of Figure 8, the inductors are expressed in terms of the circuit components as follows:

$$L_1 = \frac{R_5 R_7 R_8 C_3}{R_6}; \qquad L_2 = \frac{R_9 R_{11} R_{12} C_4}{R_{10}}. \tag{9}$$

For the following set of the parameters $R_5 = 300\,\Omega$, $R_6 = 7.5\,\text{K}\Omega$, $R_7 = 7.5\,\text{K}\Omega$, $R_8 = 5\,\text{K}\Omega$, and$C_3 = 10$ nF and $R_9 = 300\,\Omega$, $R_{10} = 7.5\,\text{K}\Omega$, $R_{11} = 7.5\,\text{K}\Omega$, $R_{12} = 5\,\text{K}\Omega$, and $C_4 = 10$ nF, we determine the corresponding values of the inductances: $L_1 = 15$ mH and $L_2 = 5$ mH. It is worth mentioning that the use of gyrators instead of real inductors is advantageous since it becomes possible to monitor the values of inductances over a wide range by simply adjust a resistor. Therefore, inductors (L_1 and/or L_2) could also be used as a bifurcation parameters (by varying ε_1 and/or ε_2). The other circuit components are taken as $C_1 = 18.4$ nF, $C_2 = 5.7$ nF, $R_3 = R_4 = 2.2\,\text{K}\Omega$, and $R_2 = 100\,\Omega$.

5.2. Experimental Results. Now, we wish to analyze the effects of the damping resistor R_1 (that deals with the

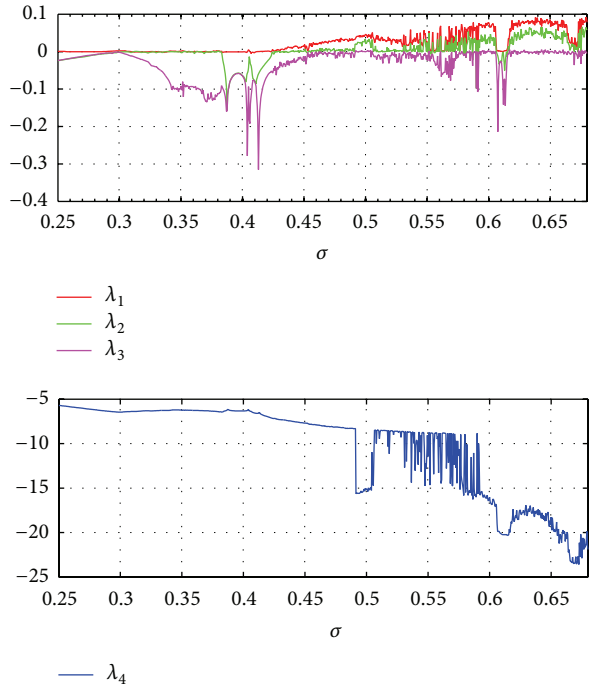

Figure 3: Lyapunov exponent spectrum versus the control parameter σ for the system parameters of Figure 2.

control parameter σ) on the dynamics of the TNC oscillator. The experimental results are obtained by slowly adjusting R_1 and plotted phase space trajectories (V_{C_1}, V_{C_2}) using a dual trace analog oscilloscope (HAMEG HM-203$_{-5}$) in the XYmode. When monitoring the resistor R_1, it is found that the experimental oscillator circuit exhibits various types of bifurcation. Indeed, for $R_1 = 4\,\mathrm{K}\Omega$, a limit cycle behavior is observed. But when R_1 decreases gradually, the following transition is obtained: periodic oscillations $\rightarrow$ torus state $\rightarrow$ chaotic oscillations $\rightarrow$ hyperchaotic oscillations $\rightarrow$ periodic oscillations $\rightarrow$ hyperchaotic oscillations. The state ww is the voltage across the capacitor C_2 as in practice it is difficult to measure through an oscilloscope the current. Some periodic windows appearing between the chaotic and hyperchaotic regimes are also noted and were only figured out numerically ($\sigma = 0.4$) using the exponential model of the diode. Figure 9 presents the result of the experimental real investigation of the TNC oscillator. From those plots, one should note that the real circuit exhibits the same bifurcation scenarios observed using theoretical methods. These results also give a good agreement between numerical and experimental results and, thereby, can be considered to validate the mathematical model (exponential model) proposed in this paper to describe the dynamic behavior of the TNC hyperchaotic oscillator.

6. Synchronization Study

In this section, we investigate the chaos synchronization of the model (4a)–(4e) with the realistic assumption of parameters uncertainty. In fact, the complex behaviors of hyperchaotic systems are believed to have much wider applications. However, they are few discussions in the literature when the parameters of the system are unknown. Moreover, in practice, some or all the parameters of the system cannot be exactly known a priori (due to temperature, external electric and magnetic fields, etc.) or may be time varying and/or inaccessible to direct measurements. Therefore, the synchronization of two uncertain chaotic systems is essential [37–42].

6.1. Design of the Slave System. For our analysis, it is assumed that the state variables of the drive system are all accessible to measurements and the system parameters are unknown.

Theorem 1. *Let the system* (4a)–(4e) *be written in the following form:*

$$\dot{X}_m = F_0(X_m) + F_1(X_m)\,\theta \tag{10a}$$

in which we have

$$\theta = (0, \varepsilon_1, \sigma, \varepsilon_2)^T;$$
$$F_0(X_m) = (z_m, 0, -x_m - \alpha\varphi(w_m), (-x_m - \alpha\varphi(w_m))/B_1(w_m))^T;$$
$$F_1(X_m) = \begin{bmatrix} 0 & 0 & 0 & 0 \\ 0 & z_m - w_m - \gamma\varphi(w_m) & 0 & 0 \\ 0 & 0 & z_m & 0 \\ 0 & 0 & \dfrac{z_m}{B_1(w_m)} & \dfrac{(-\alpha\varphi(w_m) + y_m)}{B_1(w_m)} \end{bmatrix} \tag{10b}$$

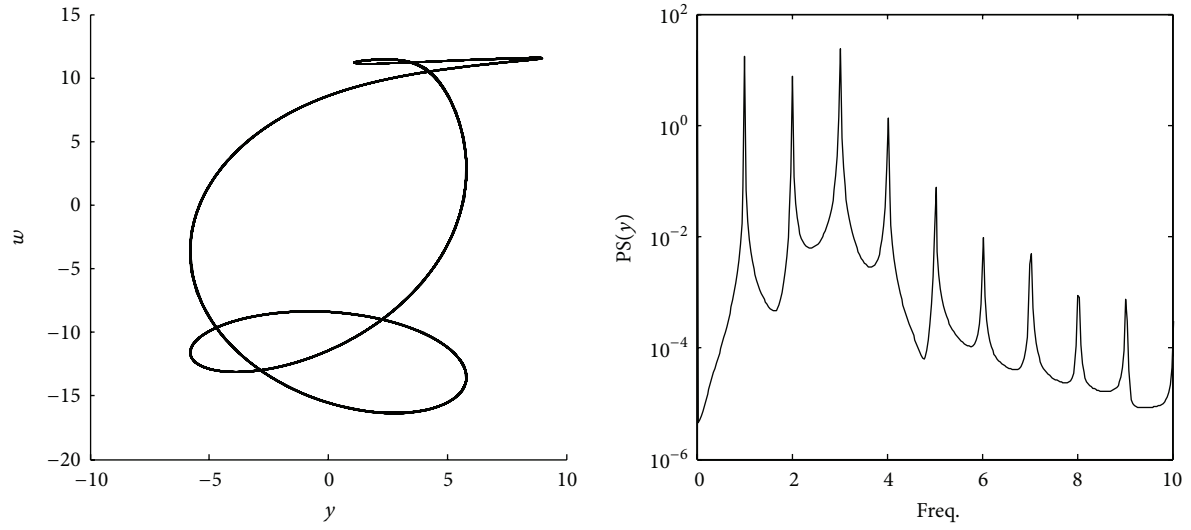

(a)

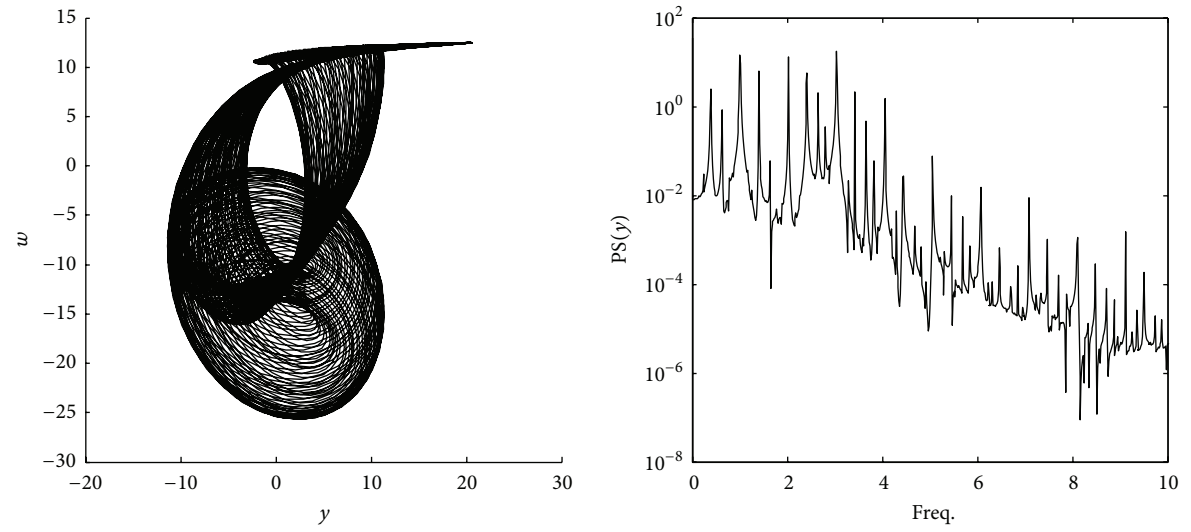

(b)

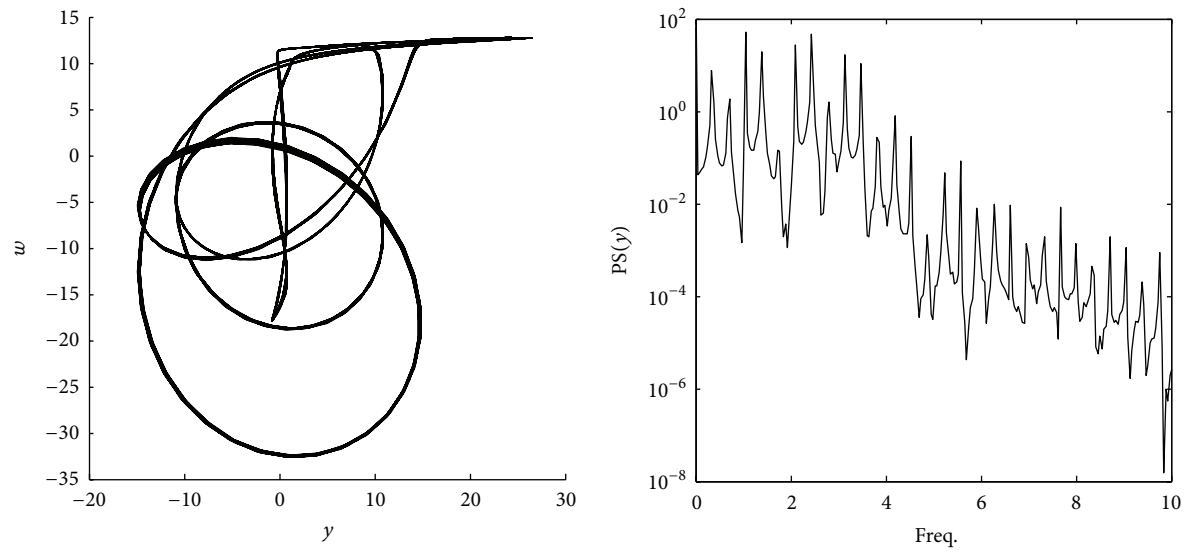

(c)

Figure 4: Continued.

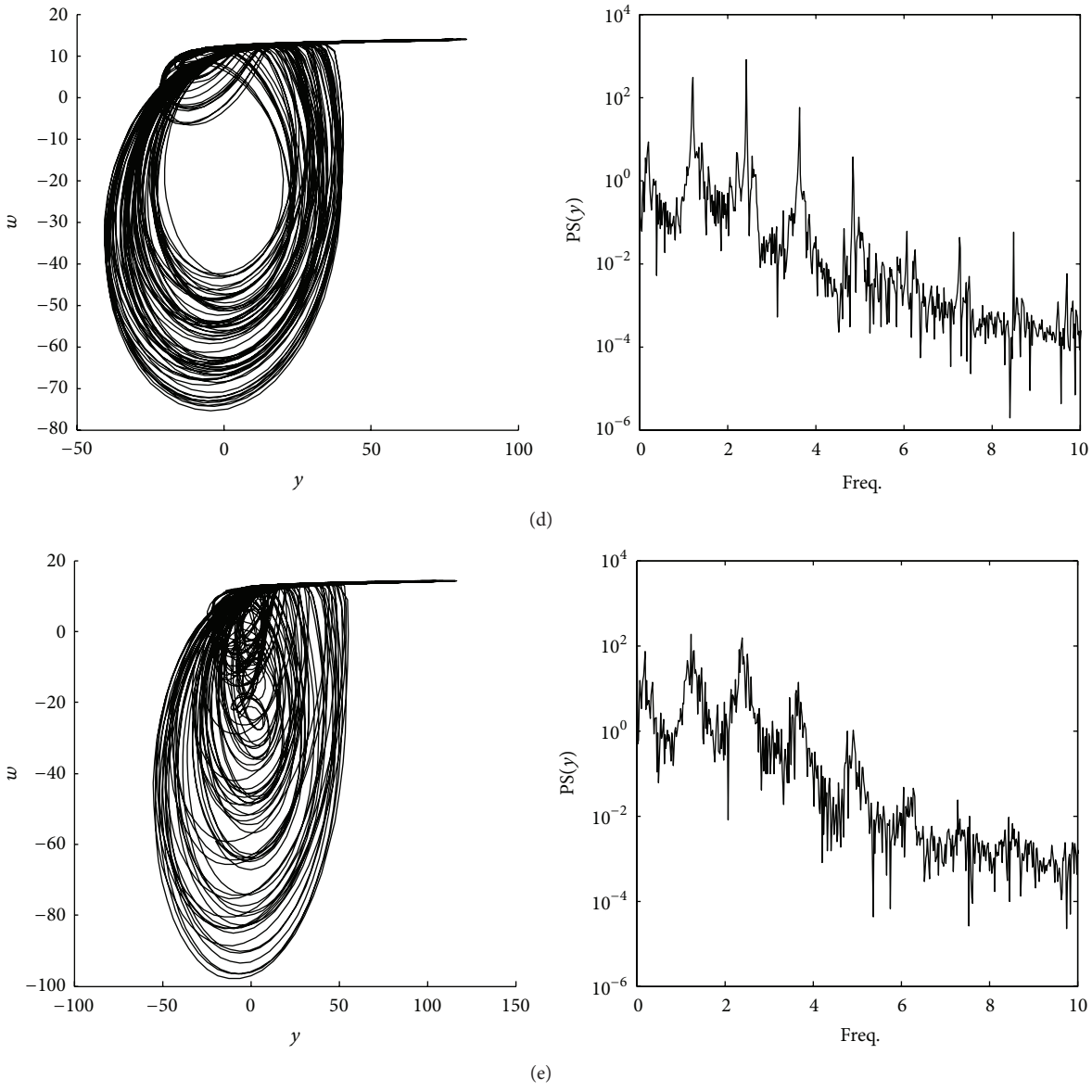

Figure 4: Numerical phase portraits of the system obtained for various values of σ: (a) periodic attractor ($\sigma = 0.25$); (b) 2D torus state ($\sigma = 0.32$); (c) periodic attractor ($\sigma = 0.4$); (d) chaos $\sigma = 0.47$; (e) hyperchaos state ($\sigma = 0.65$).

with $B_1(\omega_m) = 1 + \gamma(\varphi(\omega_m) + 1)$. *Then the corresponding response system which is given by*

$$\dot{X}_s = F_0(X_s) + F_1(X_s)\,\widehat{\theta} + u \tag{11}$$

can synchronize with the master system (10a) *and* (10b), *with the controller* u *defined as*

$$u = -\left\{e + F_0(X_s) - F_0(X_m) + \left[F_1(X_s) - F_1(X_m)\right]\widehat{\theta}(t)\right\}, \tag{12a}$$

$$\dot{\widehat{\theta}}(t) = -F_1^T(X_m)\,e, \tag{12b}$$

$$e = X_m - X_s; \qquad \widehat{\theta} = \left(0, \widehat{\varepsilon}_1, \widehat{\sigma}, \widehat{\varepsilon}_2\right), \tag{12c}$$

where $\widehat{\varepsilon}_1$, $\widehat{\sigma}$, *and* $\widehat{\varepsilon}_2$ *are the estimation of the corresponding parameters of the drive system* (10a) *and* (10b).

Proof. The error of the dynamical system can be rewritten as

$$\begin{aligned}\dot{e} &= \dot{X}_s - \dot{X}_m \\ &= F_0(X_s) + F_1(X_s)\,\widehat{\theta}(t) - e - F_0(X_s) \\ &\quad + F_0(X_m) - \left[F_1(X_s) - F_1(X_m)\right]\widehat{\theta}(t) - F_0(X_m) \\ &\quad - F_1(X_m)\,\theta = -e + F_1(X_m)\left[\widehat{\theta}(t) - \theta\right].\end{aligned} \tag{13}$$

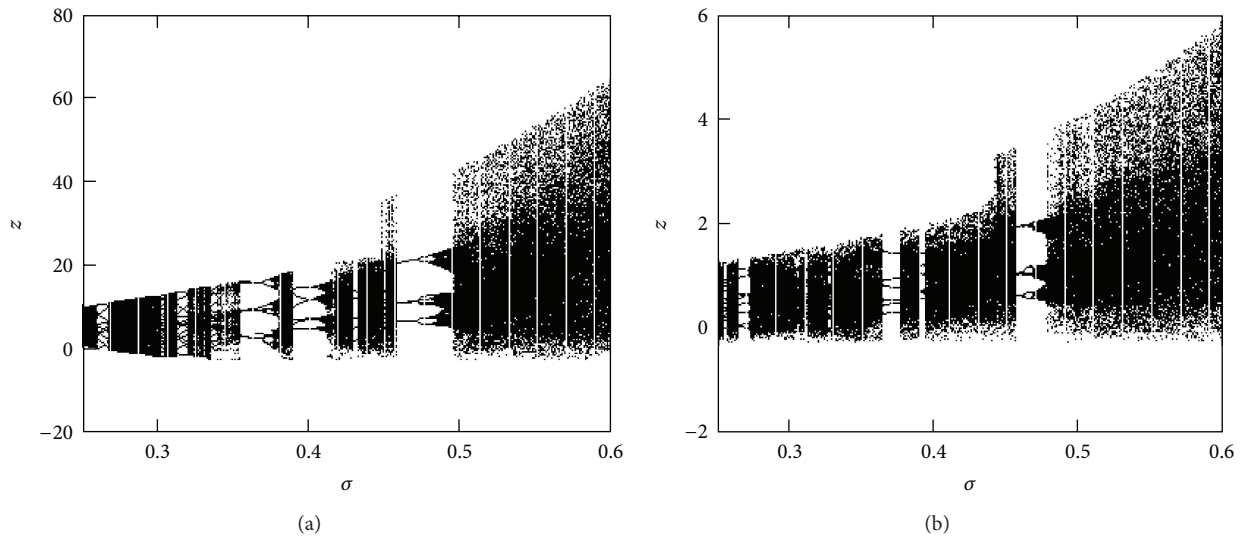

Figure 5: Comparison of the transitions exhibited by the different diode models presented in [2]. (a) Bifurcation diagram for the exponential model. (b) Bifurcation diagram for piecewise-linear model.

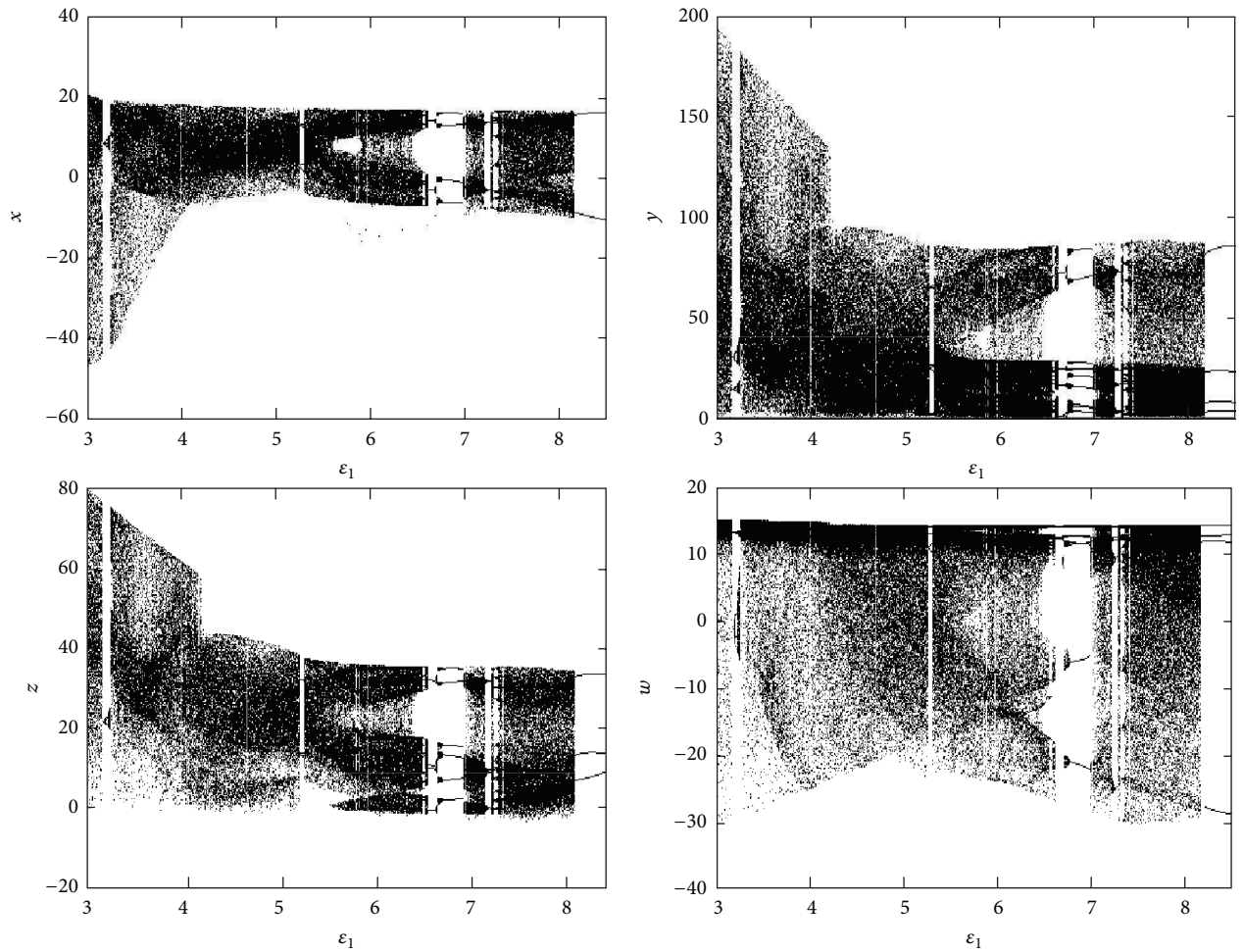

Figure 6: Bifurcation diagrams showing the coordinates x, y, z, and w in terms of the control parameter ε_1 using the system parameters of Figure 2 with $\sigma = 0.65$.

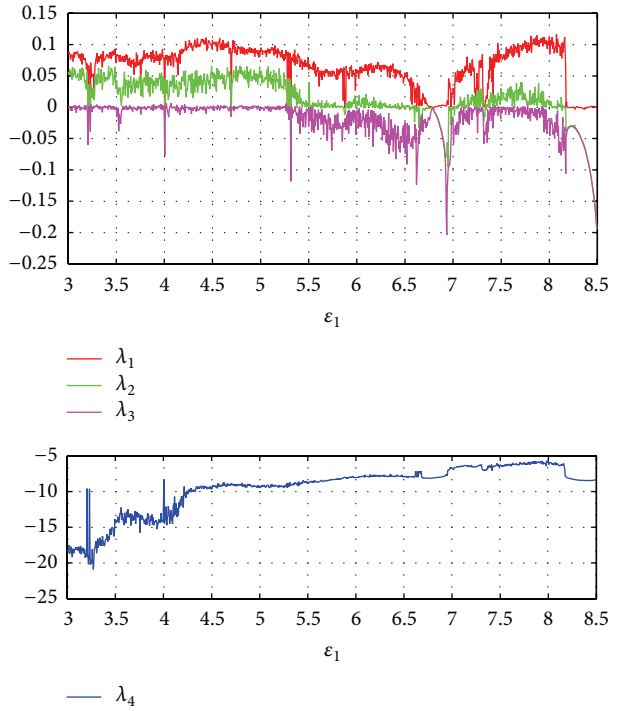

FIGURE 7: Lyapunov exponent spectrum versus the control parameter ε_1.

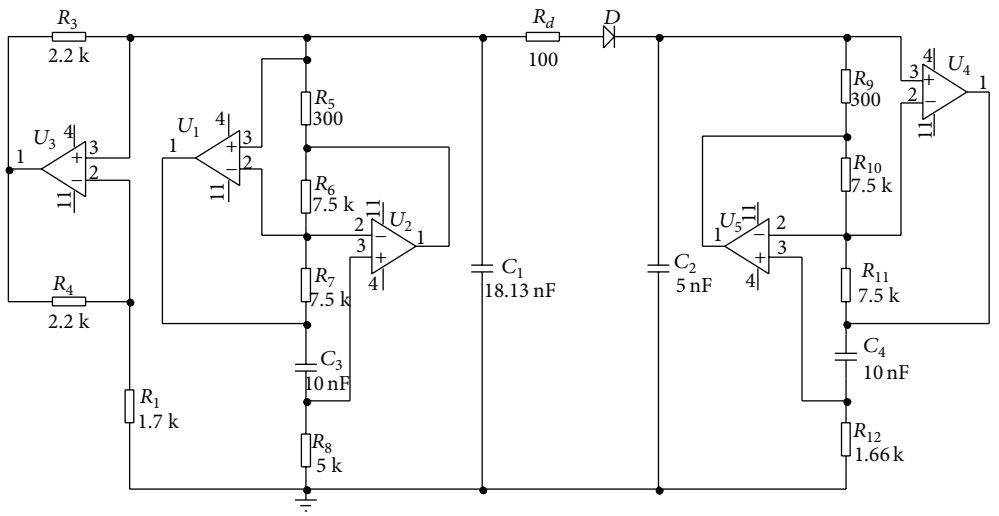

FIGURE 8: Experimental setup for measurements on the hyperchaotic oscillator. L_1 (resp., L_2) is implemented by the op amps U_1 and U_2 (resp., U_4 and U_5) based network following the approach presented in [32].

At this level, we consider the following Lyapunov function candidate:

$$V\left(e,\widehat{\theta}\left(t\right)\right)=\frac{1}{2}e^{T}e+\frac{1}{2}\left(\widehat{\theta}\left(t\right)-\theta\right)^{T}\left(\widehat{\theta}\left(t\right)-\theta\right) \tag{14}$$

whose time derivative along the trajectory is given by

$$\begin{aligned}\dot{V}&=\frac{1}{2}\left(\dot{e}^{T}e+e^{T}\dot{e}\right)\\&\quad+\frac{1}{2}\left\{\left(\dot{\widehat{\theta}}\left(t\right)\right)^{T}\left(\widehat{\theta}\left(t\right)-\theta\right)+\left(\widehat{\theta}\left(t\right)-\theta\right)^{T}\dot{\widehat{\theta}}\left(t\right)\right\}\\&=\frac{1}{2}\left(-e^{T}e+\left(\widehat{\theta}\left(t\right)-\theta\right)^{T}F_1^{T}\left(X_m\right)e\right.\\&\quad\left.-e^{T}e+e^{T}F_1\left(X_m\right)\left(\widehat{\theta}\left(t\right)-\theta\right)\right)\\&\quad+\frac{1}{2}\left(\left(\dot{\widehat{\theta}}\left(t\right)\right)^{T}\left(\widehat{\theta}\left(t\right)-\theta\right)+\left(\widehat{\theta}\left(t\right)-\theta\right)^{T}\dot{\widehat{\theta}}\left(t\right)\right)\\&=-e^{T}e\le 0.\end{aligned} \tag{15}$$

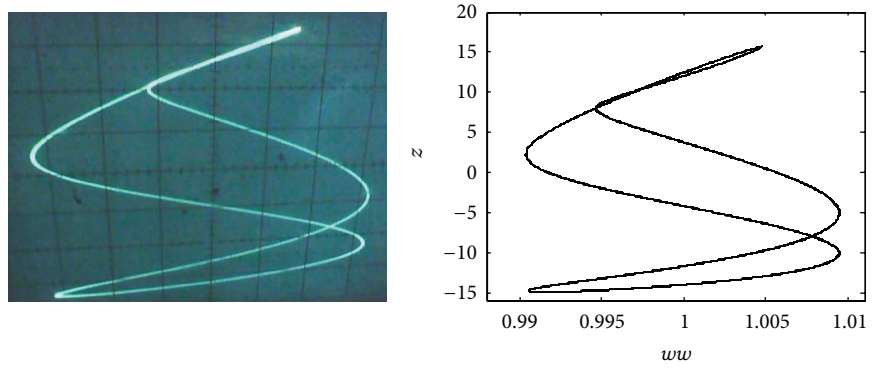

(a)

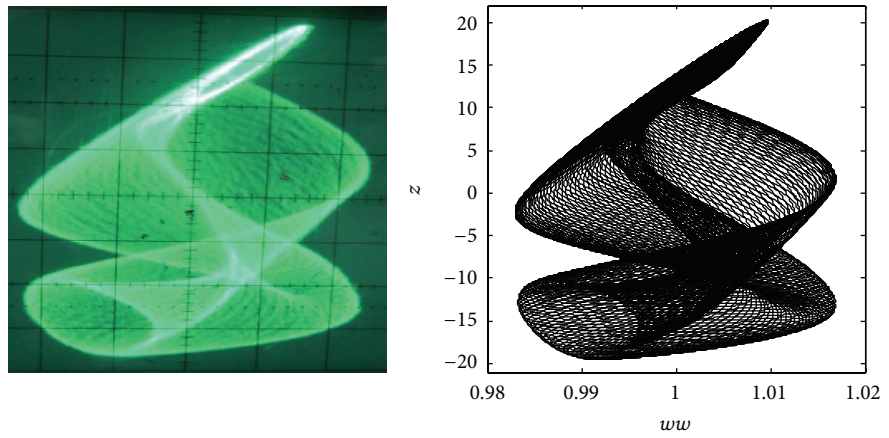

(b)

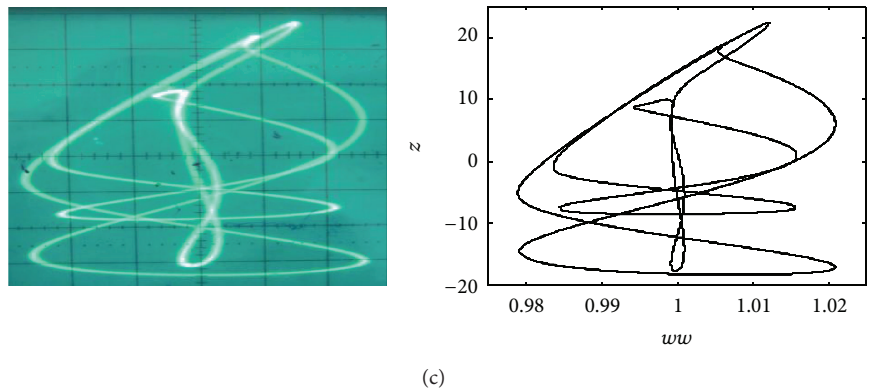

(c)

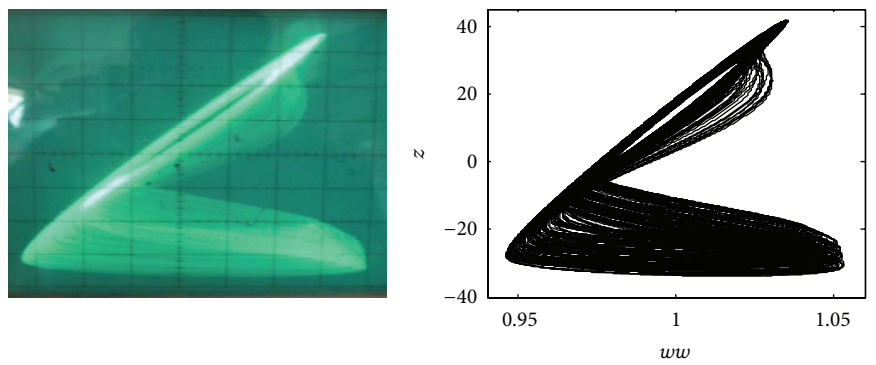

(d)

Figure 9: Continued.

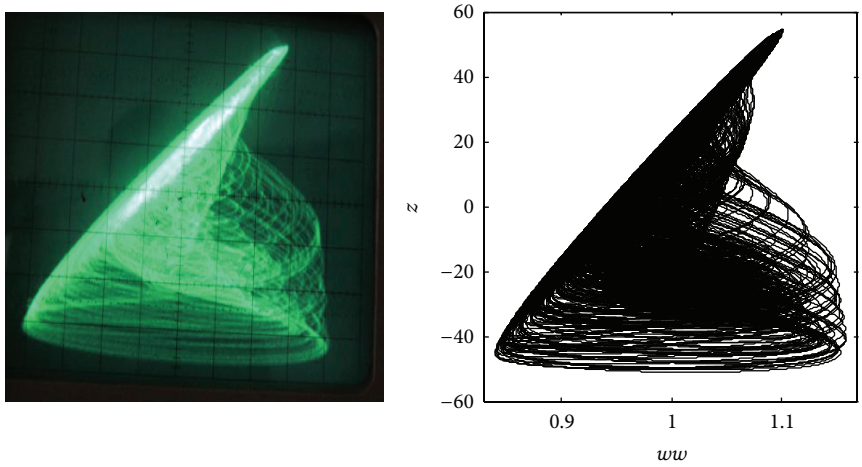

(e)

FIGURE 9: Experimental phase portraits (left hand side) obtained from the circuit using scope in Lissajou mode and their numerical correspondences (right hand side). Experimental measurements for the control parameters are (a) $R_1 = 4\,\text{k}\Omega$, (b) $R_1 = 2.82\,\text{k}\Omega$, (c) $R_1 = 2.25\,\text{k}\Omega$, (d) $R_1 = 1.92\,\text{k}\Omega$, and (e) $R_1 = 1.38\,\text{k}\Omega$.

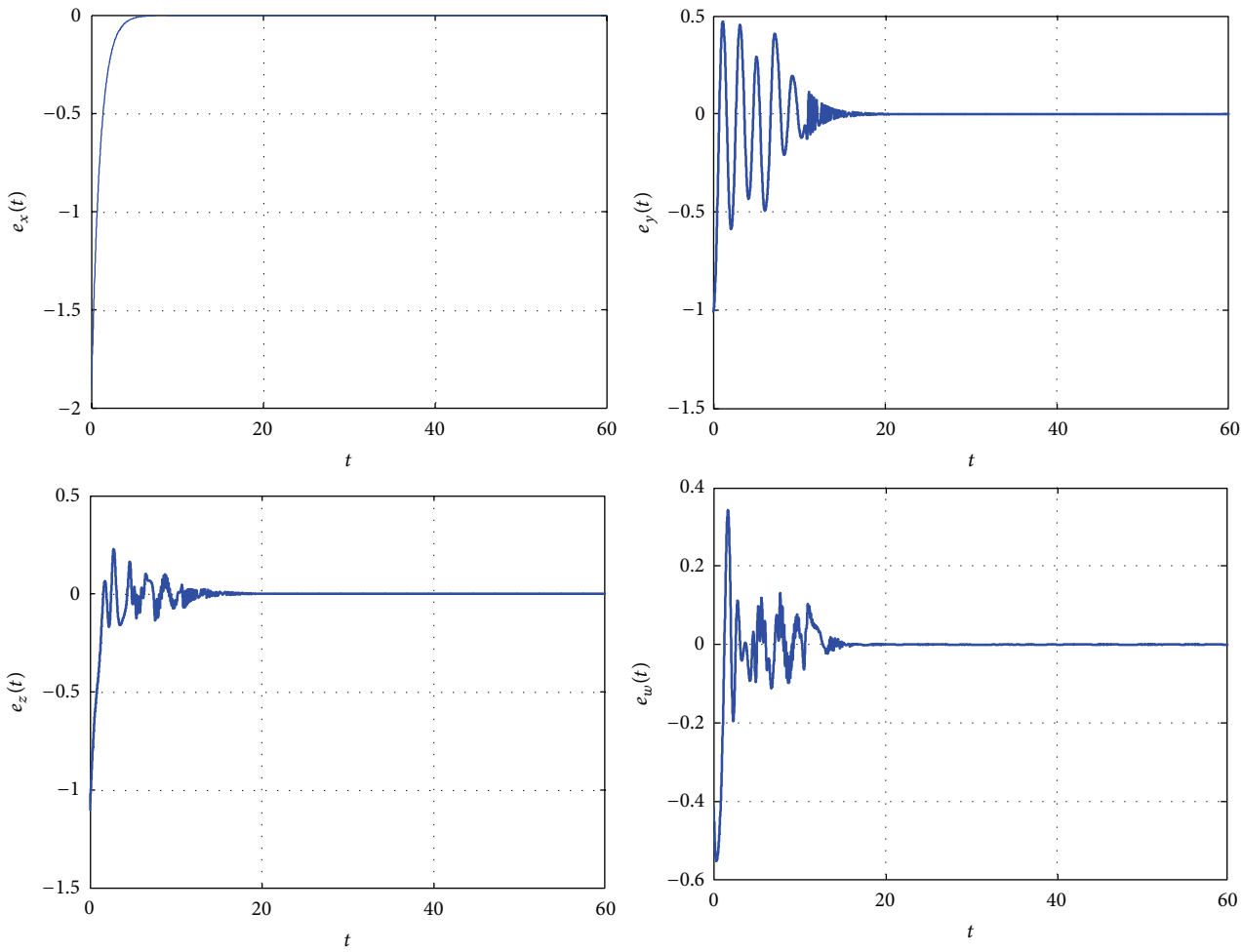

FIGURE 10: Time traces of error signals showing transition to synchronized states of the system and its observer. Initial conditions are $X_m(0) = (2, 1.2, 1, 0)^T$ and $X_s(0) = (0.1, 0.2, -0.1, -0.4)^T$. We choose the parameters of the drive system as $\varepsilon_1 = 3$, $\varepsilon_2 = 3.226$, and $\sigma = 0.65$ to ensure a hyperchaotic behavior.

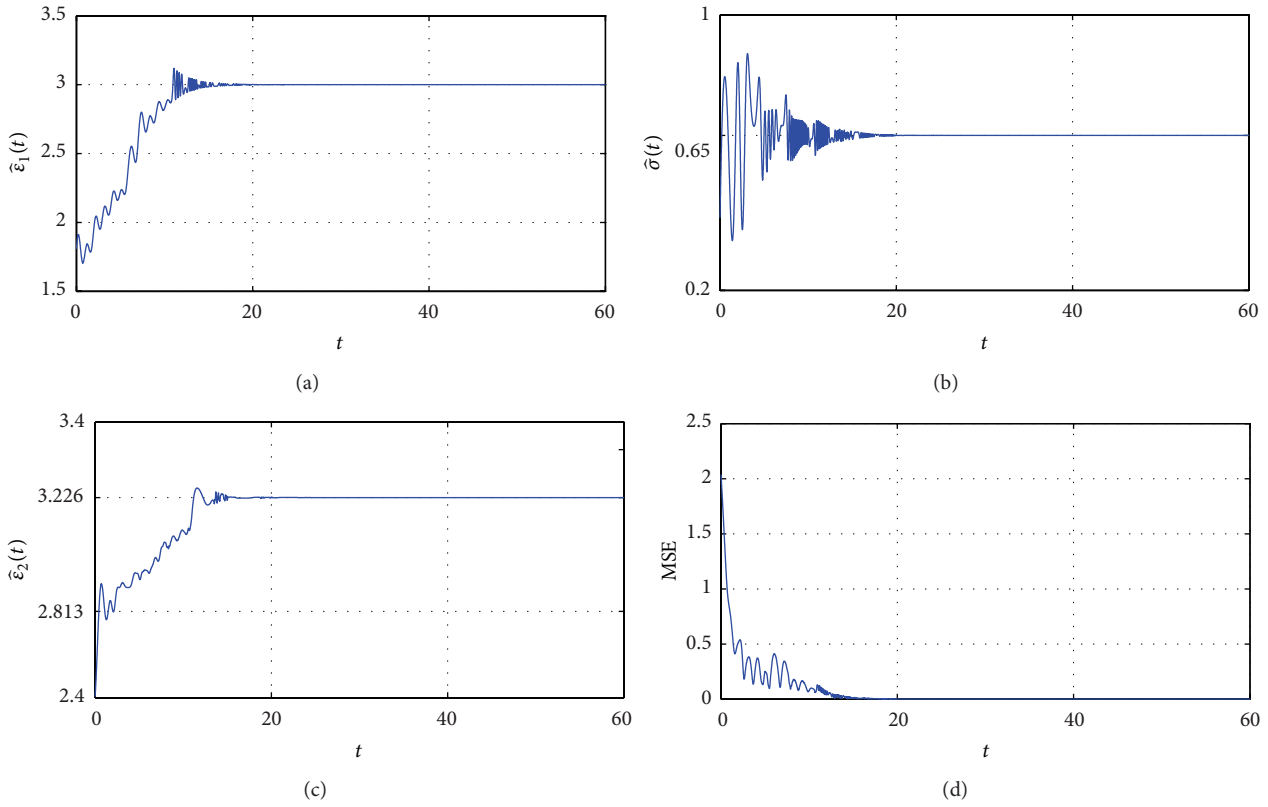

FIGURE 11: Time evolution of the estimated parameters results (a)–(c) and the mean squared error (d). Details of the captures are (a) $\widehat{\varepsilon}_1(t)$, (b) $\widehat{\sigma}(t)$, and (c) $\widehat{\varepsilon}_2(t)$.

Owing to the result (15), we conclude that $V(e, \widehat{\theta}(t))$ is a Lyapunov function of the error system and that (13) is stable at the origin, traducing the fact that $e, \widehat{\theta}$ are bounded. □

6.2. Numerical Verification. Referring to Theorem 1 above, the response system is described by the following sets of first-order differential equations:

$$\dot{\widehat{\varepsilon}}_1 = -\left(z_m - w_m - \gamma\varphi\left(w_m\right)\right) e_y, \tag{16a}$$

$$\dot{\widehat{\sigma}} = -\left(z_m e_z + \left(z_m / B_1\left(w_m\right)\right) e_w\right), \tag{16b}$$

$$\dot{\widehat{\varepsilon}}_2 = \left(\frac{\left(\alpha\varphi\left(w_m\right) - y_m\right)}{B_1\left(w_m\right)}\right) e_w, \tag{16c}$$

$$\dot{x}_s = z_m - \left(x_s - x_m\right), \tag{16d}$$

$$\dot{y}_s = \widehat{\varepsilon}_1\left(z_m - w_m - \gamma\varphi\left(w_m\right)\right) - \left(y_s - y_m\right), \tag{16e}$$

$$\dot{z}_s = \widehat{\sigma} z_m - x_m - \alpha\varphi\left(w_m\right) - \left(z_s - z_m\right), \tag{16f}$$

$$\dot{w}_s = \frac{\left(\widehat{\sigma} z_m - x_m - \alpha\varphi\left(w_m\right) - \widehat{\varepsilon}_2\left(\alpha\varphi\left(w_m\right) - y_m\right)\right)}{B_1\left(w_m\right) - \left(w_s - w_m\right)}. \tag{16g}$$

The numerical computations of (16a)–(16g) are performed using the fourth-order Runge-Kutta integration algorithm with a time step of $\Delta t = 0.005$. The initial conditions on parameters are taken as $\widehat{\varepsilon}_1(0) = 1.8$, $\widehat{\sigma}(0) = 0.4$, and $\widehat{\varepsilon}_2(0) = 2.5$. We select the parameter of the drive system as $\varepsilon_1 = 3$, $\sigma = 0.65$, and $\varepsilon_2 = 3.226$ to ensure a hyperchaotic behavior. Numerical results are shown on Figures 10 and 11. From those graphs, it can be noted that the hyperchaotic synchronization and the unknown parameters identification are achieved simultaneously after a short transient time. Obviously, this perfect synchronization may be exploited in secure communication using the technique of parameter modulation/estimation [37–39] as the system can be designed and implemented at any given frequency band depending on the values of circuit components.

7. Conclusion

In this paper, we have built a new mathematical model based on the exponential nonlinearity to examine the behavior of a simple 4D hyperchaotic electronic oscillator. This exponential model takes advantage of the PWL approximation as it provides a close form description of the oscillator's dynamics. Dynamics of the system subjected to this exponential model have been analyzed both through bifurcation diagrams, Lyapunov exponents, phase portraits, and routes to chaos. By monitoring the parameters, the system has exhibited many phase portraits with different shapes from periodic to hyperchaotic oscillations. A real physical prototype was designed and implemented on a bread board to study the

dynamics of our model. Theoretical and experimental results obtained have been compared and a very good agreement was observed. In the context of the application to secure communication, the synchronization of coupled hyperchaotic system of the model with uncertain parameters has also been studied using the recent results on adaptive control theory.

Conflict of Interests

The authors declare that there is no conflict of interests regarding the publication of this paper.

References

[1] T. Matsumoto, L. O. Chua, and K. Kobayashi, "Hyperchaos: laboratory experiment and numerical confirmation," *IEEE Transactions on Circuits and Systems*, vol. 33, no. 11, pp. 1143–1147, 1986.

[2] A. Tamaševičius, A. Namajunas, and A. Čenys, "Simple 4D chaotic oscillator," *Electronics Letters*, vol. 32, no. 11, pp. 957–958, 1996.

[3] A. Tamaševičius, A. Čenys, G. Mykolaitis, A. Namajunas, and E. Lindberg, "Hyperchaotic oscillator with gyrators," *Electronics Letters*, vol. 33, no. 7, pp. 542–544, 1997.

[4] G. Grassi and S. Mascolo, "Synchronisation of hyperchaotic oscillators using a scalar signal," *Electronics Letters*, vol. 34, no. 5, pp. 424–425, 1998.

[5] C. P. Silva and A. M. Young, "Introduction to chaos-based communications and signal processing," in *Proceedings of the 2000 IEEE Aerospace Conference*, vol. 1, pp. 279–299, March 2000.

[6] B. Cannas and S. Cincotti, "Hyperchaotic behaviour of two bidirectionally coupled Chua's circuits," *International Journal of Circuit Theory and Applications*, vol. 30, no. 6, pp. 625–637, 2002.

[7] N. Goldenfeld and L. P. Kadanoff, "Simple lessons from complexity," *Science*, vol. 284, no. 5411, pp. 87–89, 1999.

[8] R. Vicente, J. Daudén, P. Colet, and R. Toral, "Analysis and characterization of the hyperchaos generated by a semiconductor laser subject to a delayed feedback loop," *IEEE Journal of Quantum Electronics*, vol. 41, no. 4, pp. 541–548, 2005.

[9] R. Stoop, J. Peinke, J. Parisi, B. Röhricht, and R. P. Huebener, "A p-Ge semiconductor experiment showing chaos and hyperchaos," *Physica D*, vol. 35, no. 3, pp. 425–435, 1989.

[10] Y. Li, W. K. S. Tang, and G. Chen, "Hyperchaos evolved from the generalized Lorenz equation," *International Journal of Circuit Theory and Applications*, vol. 33, no. 4, pp. 235–251, 2005.

[11] Y. Li, X. Liu, G. Chen, and X. Liao, "A new hyperchaotic Lorenz-type system: generation, analysis, and implementation," *International Journal of Circuit Theory and Applications*, vol. 39, no. 8, pp. 865–879, 2011.

[12] C. K. Duan and S. S. Yang, "Synchronizing hyperchaos with a scalar signal by parameter controlling," *Physics Letters A*, vol. 229, no. 3, pp. 151–155, 1997.

[13] Z. Liu, C. Liu, M. Ho, Y. Hung, T. Hsu, and I. Jiang, "Synchronization of uncertain hyperchaotic and chaotic systems by adaptive control," *International Journal of Bifurcation and Chaos*, vol. 18, no. 12, pp. 3731–3736, 2008.

[14] J. H. Peng, E. J. Ding, M. Ding, and W. Yang, "Synchronizing hyperchaos with a scalar transmitted signal," *Physical Review Letters*, vol. 76, no. 6, pp. 904–907, 1996.

[15] A. Tamasevicius and A. Cenys, "Synchronizing hyperchaos with a single variable," *Physical Review E*, vol. 55, pp. 297–299, 1997.

[16] A. Tamaševičius, A. Čenys, A. Namajunas, and G. Mykolaitis, "Synchronising hyperchaos in infinite-dimensional dynamical systems," *Chaos, Solitons and Fractals*, vol. 9, no. 8, pp. 1403–1408, 1999.

[17] K. Murali, A. Tamasevicius, G. Mykolaitis, A. Namajunas, and E. Lindberg, "Hyperchaos system with unstable oscillators," *Nonlinear Phenomenon in Complex Systems*, vol. 3, pp. 7–10, 2000.

[18] S. Effati, J. Saberi-Nadjafi, and H. Saberi Nick, "Optimal and adaptive control for a kind of 3D chaotic and 4D hyperchaotic systems," *Applied Mathematical Modelling*, vol. 38, pp. 759–774, 2014.

[19] D. A. Miller and G. Grassi, "Experimental realization of observer-based hyperchaos synchronization," *IEEE Transactions on Circuits and Systems I*, vol. 48, no. 3, pp. 366–374, 2001.

[20] V. S. Udaltsov, J. Goedgebuer, L. Larger, and W. T. Rhodes, "Communicating with optical hyperchaos: information encryption and decryption in delayed nonlinear feedback systems," *Physical Review Letters*, vol. 86, no. 9, pp. 1892–1895, 2001.

[21] A. Buscarino, L. Fortuna, and M. Frasca, "Experimental robust synchronization of hyperchaotic circuits," *Physica D*, vol. 238, no. 18, pp. 1917–1922, 2009.

[22] C. C. Yang, "Adaptive single input control for synchronization of a 4D Lorenz-Stenflo chaotic system," *Arabian Journal for Science and Engineering*, 2013.

[23] G. Pérez and H. A. Cerdeira, "Extracting messages masked by chaos," *Physical Review Letters*, vol. 74, no. 11, pp. 1970–1973, 1995.

[24] L. Pocora, "Hyperchaos harnessed," *Physics World*, vol. 9, no. 5, p. 17, 1996.

[25] G. Qi, M. A. van Wyk, B. J. van Wyk, and G. Chen, "A new hyperchaotic system and its circuit implementation," *Chaos, Solitons and Fractals*, vol. 40, no. 5, pp. 2544–2549, 2009.

[26] L. Liu, C. Liu, and Y. Zhang, "Theoretical analysis and circuit implementation of a novel complicated hyperchaotic system," *Nonlinear Dynamics*, vol. 66, no. 4, pp. 707–715, 2011.

[27] W. Wu, Z. Chen, and Z. Yuan, "The evolution of a novel four-dimensional autonomous system: among 3-torus, limit cycle, 2-torus, chaos and hyperchaos," *Chaos, Solitons and Fractals*, vol. 39, no. 5, pp. 2340–2357, 2009.

[28] G. Grassi and S. Mascolo, "Nonlinear observer design to synchronize hyperchaotic systems via a scalar signal," *IEEE Transactions on Circuits and Systems I*, vol. 44, no. 10, pp. 1011–1013, 1997.

[29] X. Wang and Y. Wang, "Adaptive control for synchronization of a four-dimensional chaotic system via a single variable," *Nonlinear Dynamics*, vol. 65, no. 3, pp. 311–316, 2011.

[30] C. Yang, "Adaptive synchronization of Lü hyperchaotic system with uncertain parameters based on single-input controller," *Nonlinear Dynamics*, vol. 63, no. 3, pp. 447–454, 2011.

[31] A. Tamaševičius, G. Mykolaitis, A. Čenys, and A. Namajunas, "Synchronisation of 4D hyperchaotic oscillators," *Electronics Letters*, vol. 32, no. 17, pp. 1536–1538, 1996.

[32] J. Kengne, J. C. Chedjou, V. A. Fono, and K. Kyamakya, "On the analysis of bipolar transistor based chaotic circuits: case of a two-stage colpitts oscillator," *Nonlinear Dynamics*, vol. 67, no. 2, pp. 1247–1260, 2012.

[33] J. Kengne, J. C. Chedjou, G. Kenne, and K. Kyamakya, "Dynamical properties and chaos synchronization of improved Colpitts

oscillators," *Communications in Nonlinear Science and Numerical Simulation*, vol. 17, no. 7, pp. 2914–2923, 2012.

[34] A. S. Sedra and C. S. Kenneth, *Microelectronic Circuits*, Oxford University Press, New York, NY, USA, 5th edition, 2003.

[35] A. Wolf, J. B. Swift, H. L. Swinney, and J. A. Vastano, "Determining Lyapunov exponents from a time series," *Physica D*, vol. 16, no. 3, pp. 285–317, 1985.

[36] K. Giannakopoulos, T. Deliyannis, and J. Hadjidemetriou, "Means for detecting chaos and hyperchaos in nonlinear electronic circuits," in *Proceedings of the 14th IEEE International Conference on Digital Signal Processing*, pp. 951–954, 2002.

[37] H. B. Fotsin and P. Woafo, "Adaptive synchronization of a modified and uncertain chaotic Van der Pol-Duffing oscillator based on parameter identification," *Chaos, Solitons and Fractals*, vol. 24, no. 5, pp. 1363–1371, 2005.

[38] Y. Xu, W. Zhou, J. Fang, and W. Sun, "Adaptive bidirectionally coupled synchronization of chaotic systems with unknown parameters," *Nonlinear Dynamics*, vol. 66, no. 1-2, pp. 67–76, 2011.

[39] H. Adloo and M. Roopaei, "Review article on adaptive synchronization of chaotic systems with unknown parameters," *Nonlinear Dynamics*, vol. 65, no. 1-2, pp. 141–159, 2011.

[40] S. Vaidyanathan, "Analysis, control and synchronization of hyperchaotic Zhou system via adaptive control," *Advances in Computing and Information Technology*, vol. 117, pp. 1–10, 2013.

[41] X. Zhou, L. Xiong, and X. Cai, "Adaptive switched generalized function projective synchronization between two hyperchaotic systems with unknown parameters," *Entropy*, vol. 16, pp. 377–388, 2014.

[42] X. Zhou, Z. Fan, D. Zhou, and X. Cai, "Passivity-based adaptive hybrid synchronization of a new hyperchaotic system with uncertain parameters," *The Scientific World Journal*, vol. 2012, Article ID 920170, 6 pages, 2012.